

Modeling of a 6H-SiC MESFET for high-power and high-gain applications

H. Arabshahi and M. Rezaee Rokn-Abadi

Physics Department, Ferdowsi University of Mashhad, Mashhad, Iran

arabshahi@um.ac.ir

Abstract

A Monte Carlo simulation has been used to model steady state and transient electron transport in 6H-SiC field effect transistor. The simulated device geometries and doping are matched to the nominal parameters described for the experimental structures as closely as possible and the predicted I-V and transfer characteristics for the intrinsic devices show fair agreement with the available experimental data. Simulations of the effect of modulating the gate bias have also been carried out to test the device response and derived the frequency bandwidth. Value of 90 ± 10 GHz has been derived for the intrinsic current gain cut-off frequency of the 6H-SiC MESFETs.

Keywords: Steady-state, transient, cut-off frequency, frequency bandwidth.

Introduction

6H-SiC is a wide band gap semiconductor and therefore has a high breakdown field and low thermal generation rate (Brennan, 1998). These properties combined with good thermal conductivity and stability make 6H-SiC an attractive material for high power, high temperature and radiation harsh environment electronic devices. Monte Carlo simulations predict a peak electron velocity of 3×10^7 cm/s and a saturation electron velocity of 1.3×10^7 cm/s (Albrecht *et al.*, 1999). This makes possible high frequency operation of SiC devices. 6H-SiC is believed to be the most important SiC poly type (in comparison to 4C-SiC) for high reliability power field effect transistor technology (Arabshahi *et al.*, 2008) due to the higher than 4H-SiC conduction band offset with SiO₂. In this paper, we report a Monte Carlo simulation which is used to model electron transport in hexagonal 6H-SiC MESFETs. The device geometries and transport model are described and simulation results are provided.

The simulation model

Electron particles in the ensemble Monte Carlo simulation occupy non-parabolic ellipsoidal valleys in reciprocal space, and obey Boltzmann statistics. Herring-Vogt transformations are used to map carrier momenta into spherical valleys when particles are drifted scattered or cross hetero-junctions (where care has been taken to ensure that the crystal momentum in the plane of the junction is conserved across the interface). The electric field equations are solved self-consistently with the electron transport using a finite difference method (Bhupkar & Shur, 1997) and the device grid potentials are updated at each ensemble drift time step (1 femtosecond). Electrons in the bulk are scattered by ionized impurities and by bulk acoustic and non-polar optical phonon modes. Intervalley scattering by the absorption and emission of long wavelength acoustic and optic phonons have also been considered in the model. As described in detail (Brennan *et al.*, 2000) model devices are built up as a series of joined rectangular regions with the electric field cell sizes matched along the join between each region. Each region can consist of multiple layers of different alloy composition and

doping/compensation density. The 6H-SiC MESFET can be described simply by three regions (Fig. 1), representing source and drain doping implants and a central region containing the supply layers (Brennan & Brown, 2002). The field cell size used for the central region is 30 nm^2 (horizontal x vertical) but that in the high doped source and drain implants is finer (10 nm^2). Simulations of steady current characteristics have been carried out using 20000 electron particles; later simulations to derive the frequency response have required 50000 particles.

Fig.1 shows a schematic of the modeled 6H-SiC MESFET. The overall device length is $2 \mu\text{m}$ in the x-direction and the device has a $0.2 \mu\text{m}$ gate length and $0.15 \mu\text{m}$ source and drain length. The source and drain have Ohmic contacts and gate is in Schottky contact in 1 eV to represent the contact potential at Au/Pt. The source and drain regions are doped to $2 \times 10^{24} \text{ m}^{-3}$ electron concentration and the top and down buffer layers are doped to $2 \times 10^{23} \text{ m}^{-3}$ and $5 \times 10^{22} \text{ m}^{-3}$ electron concentration, respectively.

The modeled structure is divided into three regions, as indicated. Electron particles are initially distributed keeping all regions charge neutral. The location of the source and the drain implants and the top and back buffer layer are marked. Subsequent to modeling the steady state characteristics, simulations of the effect of modulating the gate bias have also been carried out, in order to test the drain current response and drive the cut-off frequency corresponding to unit current gain. The frequency response was investigated by applying truncated sinc voltage pulse to both gate contacts of the 6H-SiC MESFET. The time dependence of the voltage signal is (Donnarumma *et al.*, 2009).

$$V_{gate}(t) = V_0 + V_{amplitude} \times \frac{\sin \omega(t - T/2)}{\omega(t - T/2)} \quad (1)$$

with $\omega = 2\pi T/T_{mini}$, where V_0 is the steady gate bias upon which the modulation signal is superimposed, $V_{amplitude}$ the peak voltage during the signal, T is the duration of the signal, and T_{mini} is the duration of each minicycle within that signal; in this instance ten minicycles

Fig. 1. The two-dimensional model of 6H-SiC MESFET.

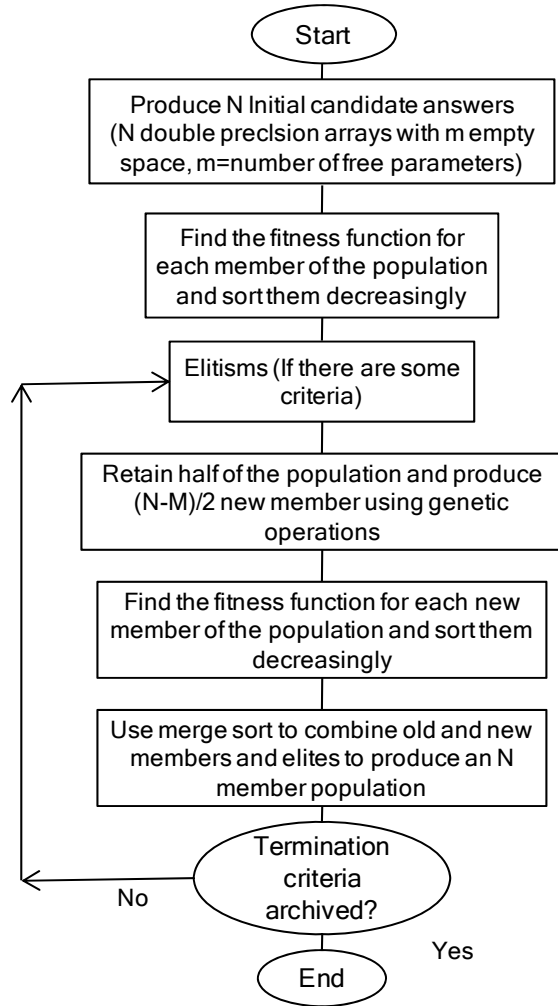


Fig. 2. Simulated current-voltage characteristics for the 6H-SiC MESFET at 300 K.

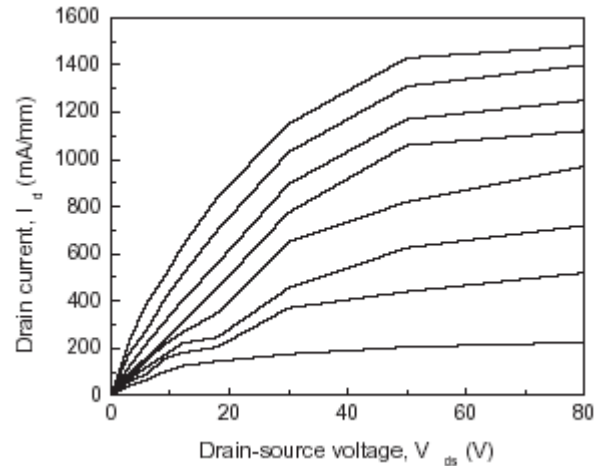


Fig. 3. Interpolated contour plot.

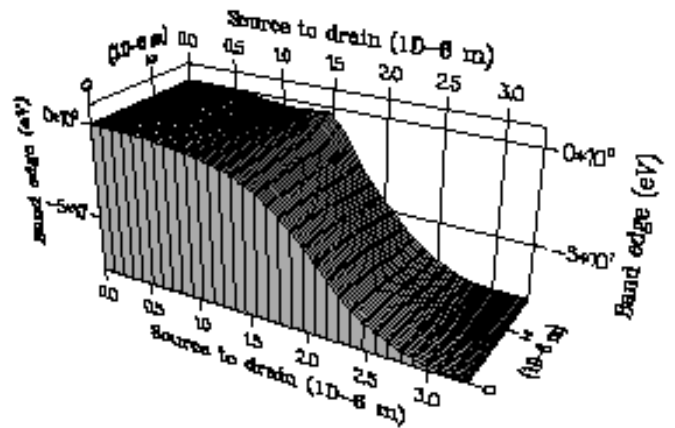


Fig.5. The simulated frequency response of 6H-SiC MESFET.

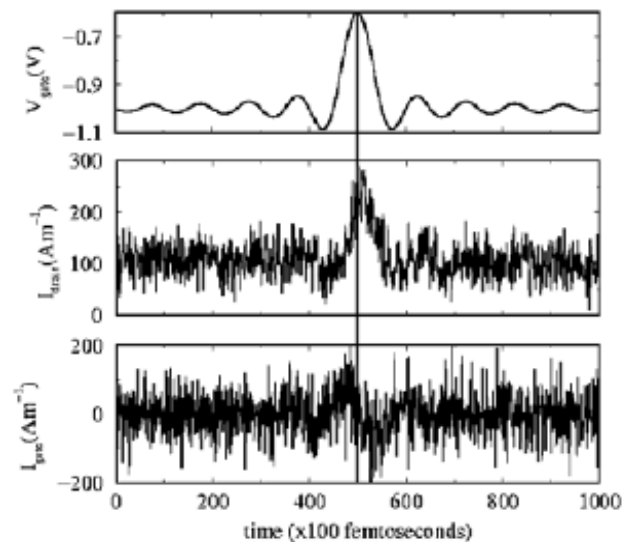
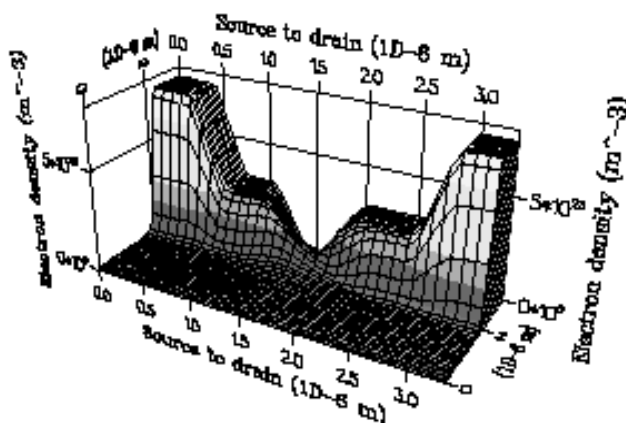


Fig. 4. Logarithmic plot.



have been used. A 100 ps duration sinc-form pulse containing ten minicycles has the specific advantage of providing a flat frequency spectrum up to 100 GHz, with 10 GHz resolution. The material parameters used in our simulation are listed in Table 1.

Simulation results

Fig. 2 shows the simulated drain current-voltage characteristic for the 6H-SiC MESFET, with the gate voltage descending from -1 V to -13 V in -2 intervals. The simulated characteristics at room temperature show good saturation behaviour with a knee voltage around 20-30 V and a saturation drain current of about 1450 mAmm^{-1} for $V_{gs}=-1 \text{ V}$. The high drain current density is encouraging for the use of 6H-SiC for high power applications. It is also clear that the device is not completely pinched-off even at large negative gate bias ($V_{gs}=-13 \text{ V}$) which is due to strong electron injection into the buffer layer at high electric fields. An increasing fraction of the drain current flows through the buffer as the drain voltage increases. Fig. 3 and 4 show the steady state Γ -valley band profile and the total electron density as a function of distance from the source when the drain-source potential drop is 20 V and the gate voltage is -1 V. Note that almost all the drain-source potential is dropped within the gate-drain region of the channel, leaving a flat potential profile near the source and drain. As electrons move towards the drain, they lose potential energy and gain sufficient kinetic energy to transfer to the upper conduction valleys where their drift velocity is reduced. Fig. 4 demonstrates the electron density through the device. The gate depletion region is clearly seen where the electron density is several orders of magnitude lower than it is near the source and drain.

Fig. 5 shows the sinc voltage signal applied to the gate, the drain current response and the gate current for the simulated 6H-SiC MESFET. In Fig. 5, the gate current (I_{gate}) is electric displacement, so resembles the derivative of the sinc voltage (V_{gate}). Note that the gate current shown is the sum of the electric displacement, occurring at the left and right hand electrodes (Fig. 1). The reproduction of the sinc pulse in the time dependence of the drain current is easy to discern, despite high frequency noise on the recorded currents, which is a direct consequence of the motion of the finite number of electron particles across the field cell grid in the simulation. The current gain has been derived as a function of frequency by taking fast Fourier transforms of the simulated drain and gate current signals, then obtaining the ratios of the coefficients of the drain and gate current transforms. The calculated cut-off frequency for the simulated device is about $90 \pm 10 \text{ GHz}$. If the data are extrapolated to the low frequency limit, the

current gain is expected to be of the order of 20 dB. From top to bottom, the figure shows the gate voltage (V_{gate}) as a function of time for a truncated pulse of duration 100 ps, the drain current response (I_{drain}) and the gate current (I_{gate}) which is electric displacement.

Conclusion

A Monte Carlo simulation was used to model steady state and transient electron transport in a 6H-SiC metal semiconductor field effect transistor. Our simulation results show that due to the high drain current density we can expect 6H-SiC devices have superior high power and high gain performance. The frequency response of the device has also been studied by applying a sinc pulse and sinusoidal signals at a range of frequencies to the gate. Due to the high intrinsic cut-off frequency ($\approx 90 \pm 10 \text{ GHz}$) the present results can also provide the useful advantages of 6H-SiC MESFET for high frequency performance.

Acknowledgements

This work is supported by the Ferdowsi university of Mashhad through a contract number 15462/2 with vice president for research and technology.

References

- Albrecht JD, Ruden PP, Limpijumnong S, Lambrecht WRL and Brennan KF (1999) High field electron transport properties of bulk ZnO. *J. Appl. Phys.* 86, 6864-6867.
- Arabshahi H, Khalvati MR and Rezaee Rokn-Abadi M (2008) Comparison of steady-state and transient electron transport in InAs, InP AND GaAs. *Modern Phys. Letts. B*, 22(17), 1695-1702.
- Arabshahi H, Khalvati MR and Rezaee Rokn-Abadi M (2008) Temperature and doping dependencies of electron mobility in InAs, AlAs and AlGaAs at high electric field application. *Braz. J. Phys.* 38(3A), 293-296.
- Bhaskar UV and Shur MS (1997) Monte Carlo calculation of velocity-field characteristics of wurtzite GaN, *J. Appl. Phys.* 82, 1649-1655.
- Brennan KF (1998) Theory of high-field electronic transport in bulk ZnS and ZnSe. *J. Appl. Phys.* 64, 4024-4030.
- Brennan KF and Brown AS (2002) Theory of modern electronic semiconductor devices, John Wiley & Sons, Inc.
- Brennan KF, Bellotti E, Farahmand M, Haralson J, Ruden PP, Albrecht JD and Sutandi A (2000) Materials theory based modeling of wide band gap semiconductors: From basic properties to devices. *Solid-State elec.* 44, 195-204.
- Donnarumma G, Wozny J and Lisik Z (2009) Monte Carlo simulation of bulk semiconductors for accurate calculation of drift velocity as a parameter for drift-diffusion, hydrodynamic models. *Materials Sci. Engg. B*, 165, 47-49.
- Farahmand M, Goano M and Ruden PP (2001) Monte Carlo simulation of electron transport in the III-nitride Wurtzite phase materials system: binaries and ternaries. *IEE Trans. Elec. Dev.* 48(3), 535-542.

Table 1. Important parameters used in our simulations for 6H-SiC material (Farahmand et al., 2001).

parameter	6H-SiC
Density ρ (kgm^{-3})	3200
Longitudinal sound velocity v_s (ms^{-1})	1373
Low-frequency dielectric constant ϵ_s	9.7
High-frequency dielectric constant ϵ_∞	6.5
Acoustic deformation potential (eV)	15
Polar optical phonon energy (eV)	0.012
Γ -valley effective mass (m)	0.28
Γ -valley nonparabolicity (eV^{-1})	0.323